Applied Physics Letters

Dynamics and interactions of magnetically driven colloidal microrotors

Cite as: Appl. Phys. Lett. **120**, 081601 (2022); https://doi.org/10.1063/5.0076574
Submitted: 26 October 2021 • Accepted: 05 February 2022 • Published Online: 22 February 2022

Raúl Josué Hernández Hernández, Thomas M. Fischer and Pietro Tierno

COLLECTIONS

EP This paper was selected as an Editor's Pick

AIP Publishing

Applied Physics Letters ARTICLE scitation.org/journal/apl

Dynamics and interactions of magnetically driven colloidal microrotors

Cite as: Appl. Phys. Lett. **120**, 081601 (2022); doi: 10.1063/5.0076574
Submitted: 26 October 2021 · Accepted: 5 February 2022 ·
Published Online: 22 February 2022

View Online Export Citation CrossMark

Raúl Josué Hernández Hernández,[1,2] Thomas M. Fischer,[3] and Pietro Tierno[1,2,4,a)]

AFFILIATIONS

[1]Departament de Física de la Matèria Condensada, Universitat de Barcelona, 08028 Barcelona, Spain
[2]Universitat de Barcelona Institute of Complex Systems (UBICS), Universitat de Barcelona, 08028 Barcelona, Spain
[3]Department of Physics, University of Bayreuth, Universitaätsstr. 30, 95447 Bayreuth, Germany
[4]Institut de Nanociència i Nanotecnologia, Universitat de Barcelona, 08028 Barcelona, Spain

[a)]Author to whom correspondence should be addressed: ptierno@ub.edu

ABSTRACT

We study the pair interactions between magnetically driven colloidal microrotors with an anisotropic shape. An external precessing magnetic field induces a torque to these particles spinning them at a fixed angular frequency. When pair of rotors approach each other, the anisotropic particles interact via dipolar forces and hydrodynamic interactions (HIs) excited by their rotational motion. For applied field spinning close to the magic angle, $\vartheta_m = 54.7°$, dipolar interactions vanish and the dynamic assembly of the pair is driven only by HIs. Further, we provide a theoretical description based on the balance between dipolar forces and HIs that allow understanding the role of anisotropy on the collective dynamics. Investigating microscopic colloidal rotors and understanding their collective dynamics are important tasks for both fundamental reasons, but also to engineer similar fluid stirrers that can be readily used for precise microscale operations or as microrheological probes.

Externally controlled rotating micro-objects (rotors) that interact, assemble, or separate in viscous fluids represent a suitable model system for more complex natural phenomena. Examples span from the organization of rotating vortices of sperm cells,[1] to the assembly of Volvox algae,[2] bacterial suspensions,[3] or synchronization phenomena.[4–6] Magnetic microrotors can also be employed in different technological applications, for example, they can be used as controllable fluid mixers in microfluidic devices,[7–11] as micromachines,[12] or as "reconfigurable" micromechanical gear systems.[13–15]

At low Reynolds number (*Re*), when viscous stresses dominate over inertial one, the response of the fluid to the spinning of the rotors is instantaneous. The hydrodynamic interactions (HIs) between microscale objects can be studied in real space by using liquid dispersions of colloidal particles.[16] Recent experiments have largely focused on the interactions between couples[17–19] or ensembles[20–22] of monodisperse *spherical* particles. However, when externally rotated, two spherical particles do not exhibit the same complexity of HIs as anisotropic bodies, since they do not require periodic flow into and out of the region between the rotors. Natural rotors are non-spherical objects, and hence, it is, important to study the effect of anisotropy on the interaction between rotors.

At low *Re*, the path of two rotors immersed in a fluid is solely determined by the geometry and the orientation of the sequence of shapes that they assume, and not by the rate at which both reorient and change shape.[23] The HIs between two rotors are non-linear[24,25] and can, in principle, cause a periodic attraction and repulsion between the couple. Thus, two non-chiral rotors cannot change their separation during one period of rotation since one half of their rotation is the chiral mirror image of the other. Symmetry together with the independence of the final result dictates the rotors to return to exactly the separation they started after each period of the motion.[26] Thus, interactions other than HIs between the rotors are needed to prevent such reciprocal motion and induce collapse or separation between them.

Here, we investigate the dynamics of two interacting magnetic microrotors made of hematite ferromagnetic ellipsoids. We use an external precessing magnetic field to induce rotational motion and tunable dipolar interactions. These interactions can be used to assemble or disassemble the couple by varying the precessing angle. When the applied field spins above the magic angle $\vartheta_m = 54.7°$, it forces attraction, and when it spins below ($\vartheta < \vartheta_m$), it forces repulsion between the rotors. Close to ϑ_m, we observe a periodic orbital motion

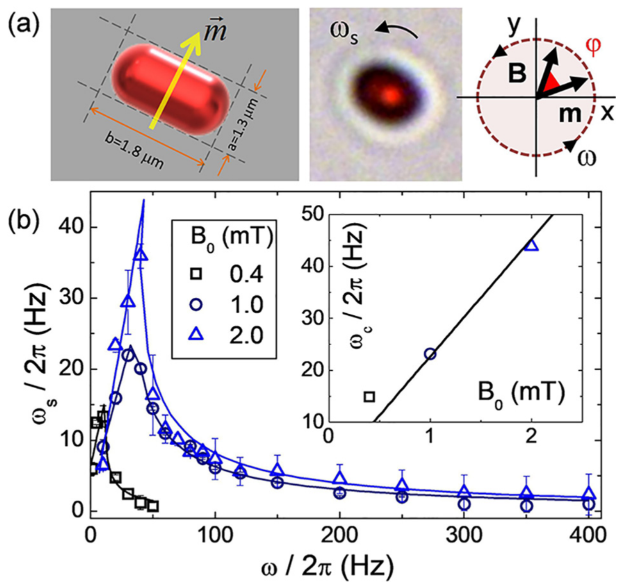

FIG. 1. (a) Left: Schematic showing one hematite particle with the direction of the permanent magnetic moment $\boldsymbol{m}$. Right: optical microscope image of one particle under a rotating field $\boldsymbol{B}$ (scheme on the right), φ denotes the phase-lag angle between $\boldsymbol{m}$ and $\boldsymbol{B}$. (b) Single particle angular spinning frequency ω_s vs driving frequency ω for three field amplitudes B_0. Scattered symbols data are experimental data, while continuous lines are regressions indicating the synchronous ($\omega < \omega_c$) and asynchronous ($\omega > \omega_c$) regimes. The inset shows the linear dependence of the critical frequency ω_c on B_0. The continuous line is a linear regression following the relationship $\omega_c = mB_0/\zeta_r$, see text.

of the pair due to HIs and the particles set at a constant separation distance. By using fast video microscopy and particle tracking routines, we quantify such interactions and put forward an analytical model that can describe the relative separation distance as a function of the shape anisotropy of both rotors.

As magnetic microrotors, we use hematite microellipsoids characterized by a long (short) axis equal to $b = 1.8 \pm 0.11 \mu$m ($a = 1.3 \pm 0.12 \mu$m), see Fig. 1(a). More details on the size distribution of these particles can be found in the supplementary material and, on the synthesis process, in previous works.[27,28] The particles are dispersed in ultra-pure water (milli-Q, Millipore) and functionalized with the surfactant sodium dodecyl sulfate (SDS), 0.12 g of SDS in 80 ml of high de-ionized water. This concentration of SDS corresponds to 5.2 mM, thus lower than the critical micelle concentration in water (8.2 mM[29]). This avoids the formation of micelles, which would decrease the adsorption of the surfactant to the particle surface. Finally, the pH of the resulting solution is adjusted to 8.5–9.5 by adding tetramethylammonium hydroxide (Sigma-Aldrich). As shown in Fig. 1(a), the particles are characterized by a small, permanent dipole moment $m \sim 2.3 \times 10^{-16}\,\mathrm{A\,m^2}$ oriented along the direction perpendicular to the particle long axis b.[30] The samples are prepared by loading $\sim$10 ml of the particle suspension in a chamber composed of a previously cleaned coverslip and a microscope slide, which are separated by two parafilm stripes and sealed with grease.

The external magnetic fields are generated by a set of magnetic coils arranged on the stage of an optical microscope (Eclipse Ni, Nikon). The latter is equipped with an oil immersion objective ($100\times$ NA = 1.3 or $40\times$ NA = 0.75, Nikon) with an additional $0.45\times$ TV lens before the camera to increase the field of view. Four coils are arranged by pairs perpendicular to each other and connected to a power amplifier (AMP-1800, Akiyama) driven by an arbitrary waveform generator (TGA12104, Aim-TTi). An additional fifth coil is placed below the sample stage connected to an independent power supply (TTi El 302) to apply a static magnetic field along an axis ($\hat{\boldsymbol{z}}$), perpendicular to the sample plane ($\hat{\boldsymbol{x}}, \hat{\boldsymbol{y}}$). Prior to the experiments, we use a teslameter (FM 205, Projekt Elektronik GmbH) to calibrate the field amplitude and its homogeneity at the particle location. Videos of the particles are recorded with a CMOS camera (AC640-Basler) working at 100 fps, and the particle positions are extracted using tracking routines.[31] More details on the experimental set-up are given in the supplementary material.

Once in water, the hematite ellipsoids sediment toward the bottom of the experimental chamber due to density mismatch. The presence of the surfactant on the particles surface prevents them to irreversibly stick to the glass substrate due to attractive Van der Waals interactions. Above the glass surface, the hematite ellipsoids are quasi two dimensionally confined, showing thermal fluctuations. From the particle positions, we extract the mean square displacement (MSD) and find a diffusive motion with a diffusion coefficient, $D = 0.073\,\mu\mathrm{m^2 s^{-1}}$; more details are given in the supplementary material.

We start to characterize the dynamics of the individual microrotors by using an in-plane rotating magnetic field with amplitude B_0 and angular frequency ω, $\boldsymbol{B} = B_0(\cos(\omega t)\hat{\boldsymbol{x}} - \sin(\omega t)\hat{\boldsymbol{y}})$. Single particles spin with angular velocity ω_s due to the magnetic torque $\tau_m = |\boldsymbol{m} \times \boldsymbol{B}| = mB \sin\varphi$, which balances the viscous torque arising from the rotation in water, $\tau_v = -\zeta_r \dot{\beta}$. Here, φ is the phase-lag angle between $\boldsymbol{B}$ and $\boldsymbol{m}$, see schematic in Fig. 1(a), $\beta = \omega t - \varphi$, and ζ_r is the rotational friction of the ellipsoid in water. The torque balance equation in the overdamped limit leads to the dynamic equation, $\dot{\varphi} = \omega - \omega_c \sin\varphi$, which predicts two dynamic regimes separated by a critical frequency ω_c, as observed in Fig. 1(b). For $\omega < \omega_c$, the rotation is phase locked with the driving field, and φ is a constant, $\omega_s = \alpha\omega$, being α is a pre-factor. In contrast, when $\omega > \omega_c$, the particle enters the asynchronous regime, where φ increases with ω, and the average rotation of the rotor ω_s decreases as $\omega_s = \alpha\omega[1 - \sqrt{1 - (\omega/\omega_c)^2})]$. As shown in the inset of Fig. 1(b), the critical frequency scales linearly with the applied field, $\omega_c = mB_0/\zeta_r$. From the linear regression, we find that $\zeta_r = (1.61 \pm 0.13) \times 10^{-21}\,\mathrm{N\,s\,m}$, similar to previous values obtained for paramagnetic ellipsoids.[32]

The complex dynamics of pair of microrotors result from the balance between magnetic dipolar forces and HIs excited by their rotary movement. We expect stronger HIs than spherical rotors[33] due to the anisotropic shape, which will create a stronger vortex flow.[34] To investigate such interactions, we choose to apply a precessing magnetic field, which allows tuning the dipolar forces from attractive to repulsive.[35,36] Such a field reads as

$$\boldsymbol{B} = B[\cos\vartheta \hat{\boldsymbol{z}} + \sin\vartheta(\cos(\omega t)\hat{\boldsymbol{x}} - \sin(\omega t)\hat{\boldsymbol{y}})], \qquad (1)$$

where ϑ is the precession angle and $B_0 = B\sin\vartheta$ is the in-plane component, Fig. 2(a). The time average dipolar forces between two equal point dipoles with magnetic moments $\boldsymbol{m}$ on the same plane and at distance r read as

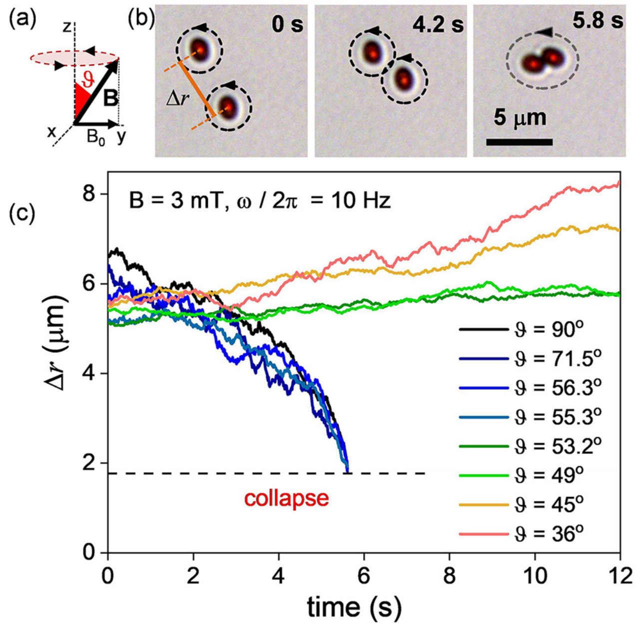

FIG. 2. (a) Schematic of the precessing magnetic field with in-plane component B_0 and precession angle ϑ. (b) Sequence of snapshots showing the collapse of two rotating hematite particles driven by a precessing field with frequency $\omega/(2\pi) = 10$ Hz, $B = 3$mT, and $\vartheta = 90°$. (c) Interparticle distance Δr between two rotors vs time t for different precession angle ϑ ($\omega/(2\pi) = 10$ Hz, $B = 3$mT).

$$\langle U_{dd}(r,\vartheta)\rangle = -\frac{\mu_0 m^2}{4\pi}\left(\frac{3\cos^2\vartheta - 1}{r^3}\right) = -\frac{\mu_0 m^2}{2\pi}\frac{P_2(\cos\vartheta)}{r^3}, \quad (2)$$

being μ_0 is the magnetic permeability of the medium (water) and $P_2(\cos\vartheta)$ is the Legendre polynomial of the first kind and second order. Thus, for a field with precession angle $\vartheta < \vartheta_m = 54.7°$, $U_{dd} > 0$ and the rotors magnetically repel, while for $\vartheta > \vartheta_m$, $U_{dd} < 0$ and they attract forming small rotating dimers, as shown in the sequence of image in Fig. 2(b).

We then perform a series of experiments by keeping fixed the driving frequency to $\omega/(2\pi) = 10$ Hz, thus when the rotors are in the synchronous regime, and by varying $\vartheta \in [36, 90]°$, Fig. 2(c). For $\vartheta \geq 55.3°$, all rotors are observed to approach each other and collapse into a rotating cluster, while for $\vartheta \in [49, 55]°$, thus near ϑ_m, the couple separates and keeps rotating at a constant separation distance of $\Delta r \sim 6\mu$m. In this situation, magnetic interactions are negligibly small, and the particles in the pair circulate one around the other as they are dragged by the flow field generated by the neighboring rotor. Now the dynamic selfassembly of the rotors is purely dictated by HIs. Decreasing further $\vartheta < 49°$ raises the strength of the repulsive dipolar forces, and the particles separate further, $\Delta r > 8\mu$m.

If we consider a pair of passive, spherical point rotors, the couple will form stable hydrodynamic bound state with constant separation distance and rotating around their center of mass with a collective angular velocity $\boldsymbol{\omega}_p = \tau_m/(4\pi\eta\Delta r^3)\hat{\boldsymbol{z}}$, being τ_m is the applied magnetic torque and η is the viscosity of the dispersing medium.[37,38] Effectively, we find that once formed at $\vartheta = 55.26$, the mean angular velocity of the pair decreases algebraically with the distance as $\omega_p \sim \Delta r^{-3}$, Fig. 3. From the analysis of different trajectories, we can extract the magnetic torque applied to each particle as $\tau_m = (1.2\pm0.3)\times10^{-19}$N mT^{-1}, which is in good agreement with that calculated directly using the magnetic torque equation.

The interaction between the rotating hematite particles is a complex interplay between magnetic dipolar forces and the shape anisotropy, which induces HIs along the separation of the particle centers, Δr. The mechanism of HIs between the anisotropic rotors can be explained by considering the periodic part of the dipolar interactions and the periodic flux in the region between the ellipsoids. Fluid is expelled from such region when the long axis rotates toward the line of separation, while it reenters the region when the long axis rotates toward a transversal orientation. Both situations repeat twice during a full field cycle, and the flux causes periodic (frequency 2ω) oscillations of the pressure. The mobility matrix that relates force and torque to speed and angular velocity for our system can be written as

$$\begin{pmatrix} \dot{\Delta r} \\ \dot{\varphi} \\ \dot{\varphi}_1 \\ \dot{\varphi}_2 \end{pmatrix} = \bar{M}\begin{pmatrix} F_{12} \\ \tau \\ \tau_1 \\ \tau_2 \end{pmatrix}, \quad (3)$$

where $F_{12} = \frac{\mu_0 m^2[P_2(\cos\vartheta)+P_2^2(\cos\vartheta)\cos(2(\varphi_1-\varphi))]}{12\pi r^4}$ denotes the dipolar interaction force between the rotors, τ, τ_1, and τ_2 are the total and individual magnetic torques, and φ, φ_1, and φ_2 are the corresponding phase-lag angles, see inset in Fig. 4. Further, $\bar{M}$ is the mobility tensor that depends on the conformations (Δr, $\varphi_1 - \varphi$, $\varphi_2 - \varphi$, ϑ_1, ϑ_2) of the rotors. We approximate the leading dependencies of the symmetric mobility matrix on the conformation by $M_{rF} = 1/6\pi\eta a$, $M_{r\tau} = 0$, $M_{r\tau_i} = a\epsilon^2\sin^2\vartheta_i\sin(2[\varphi_i - \varphi])/6\pi\eta r^3$, $M_{\varphi_i\tau_i} = 1/8\pi\eta a^3$, and $M_{\varphi\tau} = 1/3\pi\eta a r^2$, where a is the mean radius of the rotor, ϵ is the eccentricity of the rotor shape, and we assume that the rotor orientation to be locked to the magnetic field ($\vartheta_i = \vartheta$, $\varphi_i = \omega t$). The two rotors are circling around their centers of mass with frequency ω_p, and all other

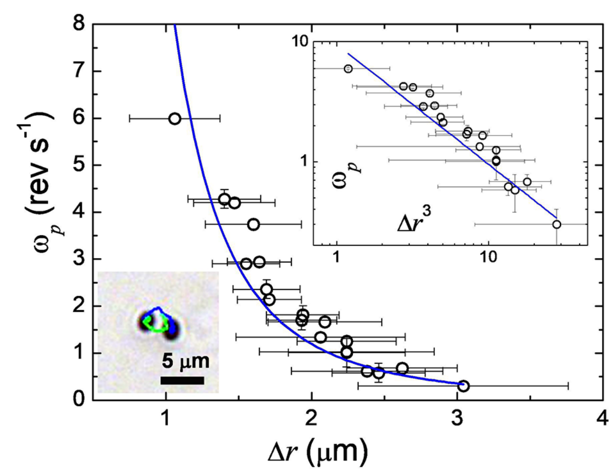

FIG. 3. Collective angular velocity ω_p of a pair of microrotors assembled by a precessing field with $f = 10$ Hz, $B = 2.1$ mT, and $\vartheta = 55.3°$ vs separation distance Δr. Scattered points are experimental data, while continuous blue line is a fit to the data with $\omega_p = \alpha/\Delta r^3$ and $\alpha = 7.1\pm0.3$rev μm^{2}s^{-1}. Top inset shows the log-log plot of ω_p vs Δr^3. Bottom inset displays a microscope image of a pair of rotors with superimposed the particle trajectories.

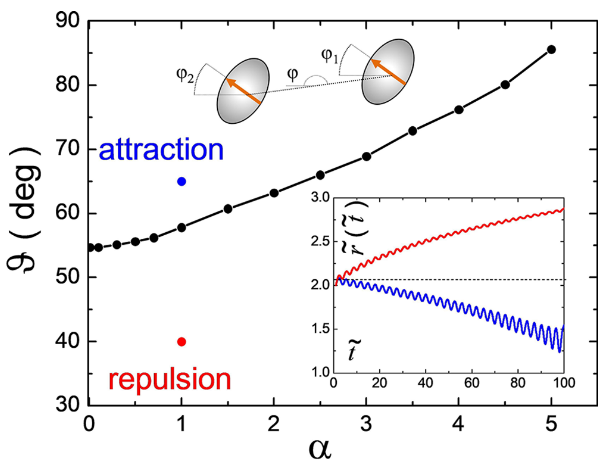

FIG. 4. Threshold between the attractive and repulsive behavior as a function of the anisotropy parameter α and the precession angle ϑ. Top inset shows a scheme of two interacting microrotors with phase lag angles $\varphi_{1,2}$. Bottom inset shows the normalized separation distance $\tilde{r}(\tilde{t})$ vs $\tilde{t}$ calculated for the precession angles $\vartheta = 40°$ (red) and $\vartheta = 60°$ (blue) and anisotropy parameter $\alpha = 1$.

non-diagonal elements of the mobility matrix are assumed to vanish. The mobility coefficient, $M_{r\tau}$, arises due to the fact that liquid needs to flow out or needs to enter the region between the two rotors when the particle orientation changes from one major axis of the hematite particle aligned with the separation to the other. Hence, we find the following differential equation:

$$\dot{\tilde{r}} = \frac{\left[\dfrac{P_2(\cos\vartheta)}{P_2^2(\cos\vartheta)} + \cos(2\tilde{t})\right]}{\tilde{r}^4} + \alpha^2\frac{\sin 2\tilde{t}}{\tilde{r}^3}, \qquad (4)$$

where we use adimensional units with $\tilde{t} = [\omega - \omega_p]t$, $\tilde{r} = \Delta r/l$ with $l = \sqrt[5]{72\pi^2\eta(\omega-\omega_p)a/\mu_0 m^2 P_2^2(\cos\vartheta)}$ and $\alpha = 2a^2\epsilon\sin\vartheta_i/\sqrt{3}l^2$. A numerical solution of Eq. (4) yields an oscillatory behavior of the separation on short time scales. On longer time scales, the equation predicts a separation for small precession angle ϑ and an attraction for larger precession angles. Figure 4 shows a phase diagram of the long time behavior as a function of the anisotropy parameter $\alpha \sim \varepsilon$ and the precession angle ϑ. The line separating attractive from repulsive interaction starts at the magic angle $\vartheta_m = 54.7°$ and zero anisotropy. Then, it monotonously increases with the parameter α, thus the shape anisotropy of the rotors. This implies that increasing the particle anisotropy raises the strength of HIs producing a shift of the magic angle toward higher values.

In conclusion, we have investigated the non-equilibrium dynamics of pair of interacting magnetic microrotors driven by an external precessing magnetic field. We show that by tuning the precession angle, one can control the assembly of the pair and reduce the effect of magnetic dipolar interactions in favor of hydrodynamic ones. The controlled stirring of anisotropic, elongated particles in viscous fluids may find several applications apart from that of fluid mixers. For example, magnetic nanorods have been used to measure the rheological properties of monolayers at the water/air interface.[39–42] When compared to the hematite particles, both type of particles should generate similar vortical flow when torque by a rotating magnetic field. However, the smaller lateral size of the nanorods will make more difficult their visualization under optical microscopy. In comparison with macroscopic rheometers, the small size of these rheological probes increases the sensitivity of the measurement while reducing the amount of material to be investigated. In this context, most of the studies so far have investigated the dynamics of single rotors in viscoelastic fluids. Thus, a potential future direction of this work could be to test how the dynamics of pair of rotors are altered by a complex non-Newtonian medium.

See the supplementary material for additional details on the experimental system, the measurements of the long and short axes of the hematite ellipsoids, and the diffusive properties of these particles.

We thank Helena Massana-Cid for experimental advice and Gaspard Junot for providing SEM images of the particles. This work received funding from the European Research Council (ERC) under the European Union's Horizon 2020 research and innovation programme (Grant Agreement No. 811234). P.T. acknowledges support from MCIU (No. PID2019-108842GB-C21) and the Program ICREA "Académia."

AUTHOR DECLARATIONS

Conflict of Interest

The authors declare no conflict of interest.

DATA AVAILABILITY

The data that support the findings of this study are available from the corresponding author upon reasonable request.

REFERENCES

[1] I. H. Riedel, K. Kruse, and J. Howard, "A self-organized vortex array of hydrodynamically entrained sperm cells," Science **309**, 300–303 (2005).
[2] K. Drescher, K. C. Leptos, I. Tuval, T. Ishikawa, T. J. Pedley, and R. E. Goldstein, "Dancing volvox: Hydrodynamic bound states of swimming algae," Phys. Rev. Lett. **102**, 168101 (2009).
[3] C. J. Pierce, H. Wijesinghe, E. Mumper, B. H. Lower, S. K. Lower, and R. Sooryakumar, "Hydrodynamic interactions, hidden order, and emergent collective behavior in an active bacterial suspension," Phys. Rev. Lett. **121**, 188001 (2018).
[4] R. D. Leonardo, A. Búzás, L. Kelemen, G. Vizsnyiczai, L. Oroszi, and P. Ormos, "Hydrodynamic synchronization of light driven microrotors," Phys. Rev. Lett. **109**, 034104 (2012).
[5] M. Theers and R. G. Winkler, "Synchronization of rigid microrotors by time-dependent hydrodynamic interactions," Phys. Rev. E **88**, 023012 (2013).
[6] J. Kotar, L. Debono, N. Bruot, S. Box, D. Phillips, S. Simpson, S. Hanna, and P. Cicuta, "Optimal hydrodynamic synchronization of colloidal rotors," Phys. Rev. Lett. **111**, 228103 (2013).
[7] A. Terray, J. Oakey, and D. W. M. Marr, "Microfluidic control using colloidal devices," Science **296**, 1841–1844 (2002).
[8] S. Bleil, D. W. M. Marr, and C. Bechinger, "Field-mediated self-assembly and actuation of highly parallel microfluidic devices," Appl. Phys. Lett. **88**, 263515 (2006).
[9] T. Sawetzki, S. Rahmouni, C. Bechinger, and D. W. M. Mar, "In situ assembly of linked geometrically coupled microdevices," Science **105**, 20141–20145 (2008).
[10] B. Kavicic, D. Babic, N. Osterman, B. Podobnik, and I. Poberaj, "Magnetically actuated microrotors with individual pumping speed and direction control," Appl. Phys. Lett. **95**, 023504 (2009).
[11] J. K. Hamilton, M. T. Bryan, A. D. Gilbert, F. Y. Ogrin, and T. O. Myers, "A new class of magnetically actuated pumps and valves for microfluidic applications," Sci. Rep. **8**, 933 (2018).
[12] P. Galajda and P. Ormos, "Complex micromachines produced and driven by light," Appl. Phys. Lett. **78**, 249 (2001).

[13] J. M. K. Ng, M. J. Fuerstman, B. A. Grzybowski, H. A. Stone, and G. M. Whitesides, "Self-assembly of gears at a fluid/air interface," J. Am. Chem. Soc. **125**, 7948–7958 (2003).
[14] B. A. Grzybowski, "Self-assembling fluidic machines," Appl. Phys. Lett. **84**, 1798 (2004).
[15] B. A. Grzybowski, K. Fitzner, J. Paczesny, and S. Granick, "From dynamic self-assembly to networked chemical systems," Chem. Soc. Rev. **46**, 5647–5678 (2017).
[16] F. Martínez-Pedrero and P. Tierno, "Advances in colloidal manipulation and transport via hydrodynamic interactions," J. Colloid Interface Sci. **519**, 296–311 (2018).
[17] P. Bartlett, S. I. Henderson, and S. J. Mitchell, "Measurement of the hydrodynamic forces between two polymer-coated spheres," Philos. Trans. R. Soc., A **359**, 883 (2001).
[18] S. Martin, M. Reichert, H. Stark, and T. Gisler, "Direct observation of hydrodynamic rotation-translation coupling between two colloidal spheres," Phys. Rev. Lett. **97**, 248301 (2006).
[19] A. C. H. Coughlan and M. A. Bevan, "Rotating colloids in rotating magnetic fields: Dipolar relaxation and hydrodynamic coupling," Phys. Rev. E **94**, 042613 (2016).
[20] K. Zahn, J. M. Méndez-Alcaraz, and G. Maret, "Hydrodynamic interactions may enhance the self-diffusion of colloidal particles," Phys. Rev. Lett. **79**, 175–178 (1997).
[21] J. Santana-Solano and J. L. Arauz-Lara, "Hydrodynamic interactions in quasi-two-dimensional colloidal suspensions," Phys. Rev. Lett. **87**, 038302 (2001).
[22] A. L. Thorneywork, R. E. Rozas, R. P. A. Dullens, and J. Horbach, "Effect of hydrodynamic interactions on self-diffusion of quasi-two-dimensional colloidal hard spheres," Phys. Rev. Lett. **115**, 268301 (2015).
[23] A. Shapere and F. Wilczek, "Self-propulsion at low Reynolds number," Phys. Rev. Lett. **58**, 2051–2054 (1987).
[24] J. Happel and H. Brenner, *Low Reynolds Number Hydrodynamics* (Noordhoff, Leiden, 1973).
[25] S. Kim and S.-J. Karrila, *Microhydrodynamics* (Butterworth-Heinemann, Boston, 1991).
[26] E. M. Purcell, "Life at low Reynolds number," Am. J. Phys. **45**, 3 (1977).
[27] F. Martinez-Pedrero, A. Cebers, and P. Tierno, "Orientational dynamics of colloidal ribbons self-assembled from microscopic magnetic ellipsoids," Soft Matter **12**, 3688–3695 (2016).
[28] F. Martinez-Pedrero, H. Massana-Cid, and P. Tierno, "Assembly and transport of microscopic cargos via reconfigurable photoactivated magnetic microdockers," Small **13**, 1603449 (2017).
[29] V. Y. Bezzobotnov, S. Borbely, L. Cser, B. Farago, I. A. Gladkih, Y. M. Ostanevich, and S. Vass, "Temperature and concentration dependence of properties of sodium dodecyl sulfate micelles determined from small angle neutron scattering experiments," J. Phys. Chem. **92**, 5738–5743 (1988).
[30] F. Martinez-Pedrero, A. Cebers, and P. Tierno, "Dipolar rings of microscopic ellipsoids: Magnetic manipulation and cell entrapment," Phys. Rev. Appl. **6**, 034002 (2016).
[31] J. C. Crocker and D. G. Grier, "Methods of digital video microscopy for colloidal studies," J. Colloid Interface Sci. **179**, 298 (1996).
[32] P. Tierno, J. Claret, F. Sagués, and A. Cēbers, "Overdamped dynamics of paramagnetic ellipsoids in a precessing magnetic field," Phys. Rev. E **79**, 021501 (2009).
[33] P. Tierno, S. Schreiber, W. Zimmermann, and T. M. Fischer, "Shape discrimination with hexapole-dipole interactions in magic angle spinning colloidal magnetic resonance," J. Am. Chem. Soc. **131**, 5366–5367 (2009).
[34] I. L. Claeyst and J. F. Brady, "Suspensions of prolate spheroids in stokes flow. Part 1. Dynamics of a finite number of particles in an unbounded fluid," J. Fluid Mech. **251**, 411–442 (1993).
[35] P. Tierno, R. Muruganathan, and T. M. Fischer, "Viscoelasticity of dynamically self-assembled paramagnetic colloidal clusters," Phys. Rev. Lett. **98**, 028301 (2007).
[36] N. Osterman, I. Poberaj, J. Dobnikar, D. Frenkel, P. Ziherl, and D. Babić, "Field-induced self-assembly of suspended colloidal membranes," Phys. Rev. Lett. **103**, 228301 (2009).
[37] E. Climent, K. Yeo, M. R. Maxey, and G. E. Karniadakis, "Dynamic self-assembly of spinning particles," J. Fluids Eng. **129**, 379–387 (2007).
[38] Y. Fily, A. Baskaran, and M. C. Marchetti, "Cooperative self-propulsion of active and passive rotors," Soft Matter **8**, 3002 (2012).
[39] A. Anguelouch, R. L. Leheny, and D. H. Reich, "Application of ferromagnetic nanowires to interfacial microrheology," Appl. Phys. Lett. **89**, 111914 (2006).
[40] P. Dhar, Y. Cao, T. M. Fischer, and J. A. Zasadzinski, "Active interfacial shear microrheology of aging protein films," Phys. Rev. Lett. **104**, 016001 (2010).
[41] L. Chevry, N. K. Sampathkumar, A. Cebers, and J.-F. Berret, "Magnetic wire-based sensors for the microrheology of complex fluids," Phys. Rev. E **88**, 062306 (2013).
[42] A. Brasovs, J. Cimurs, K. Erglis, A. Zeltins, J.-F. Berret, and A. Cebers, "Magnetic microrods as a tool for microrheology," Soft Matter **11**, 2563–2569 (2015).